To appear in *Liquid Crystals*
Vol. 00, No. 00, Month 20XX, 1–19

RESEARCH ARTICLE

Influence of internal flexibility on the double glass transition in a series of odd non-symmetric liquid crystal dimers characterized by dielectric measurements.

J.A. Diego[a*], J. Sellarès[a], S. Diez-Berart[b], J. Salud[b], J.C. Cañadas[a], M. Mudarra[a], D.O. López[b], M.R. de la Fuente[c] and M.B. Ros[d]

[ab] *Departament de Física, Universitat Politècnica de Catalunya*; [a] *ESEIAAT, Colom 1, E-08222 Terrassa, Spain*; [b] *ETSEIB, Diagonal 647, E-08028 Barcelona, Spain*; [c] *Departamento de Física Aplicada II, Facultad de Ciencia y Tecnología, Universidad del País Vasco, Apartado 644, E-48080 Bilbao, Spain*; [d] *Departamento de Química Orgánica, Facultad de Ciencias, Instituto de Ciencia de Materiales de Aragón, Universidad de Zaragoza-CSIC, 50009 Zaragoza, Spain*

(*Received 00 Month 20XX; final version received 00 Month 20XX*)

Dielectric measurements (Thermally Stimulated Depolarization Currents and Broadband Dielectric Spectroscopy) have been performed near the glass transition to study the glass transition on the odd non-symmetric liquid crystal dimers of the series α-(4-cyanobiphenyl-4´-oxy)-ω-(1-pyreniminebenzylidene-4´-oxy) alkanes (CBOnO.Py) with n ranging from 3 to 9. A previous study [S. Diez-Berart et al., Materials **8** (2015) 3334] carried out in CBO11O.Py showed the presence of two glass transition temperatures, attributed to different molecular motions of the terminal groups. The study performed allows us to analyze the molecular dynamics in the rest of the series and determine the role played by the flexible spacer. Parallel and perpendicular orientations of the molecular director with regards to the probe electric field have been investigated. The low and intermediate observed relaxations are explained in the framework of Stocchero's theoretical model [M. Stocchero, J. Chem. Phys. **121** (2004) 8079] for the dielectric behaviour of non-symmetric liquid crystals dimers, as independent end-over-end rotations of each terminal semirigid unit. As the length of the spacer chain in the series of compounds decreases, the different relaxations become progressively more coupled at the glass transition. Numerical simulations of the calorimetric response from the obtained kinetic parameters show good agreement with experimental behaviour.

Keywords: dimers; glass transition; thermally stimulated discharge currents; Tool-Narayanaswamy-Moynihan model; relaxation time; broadband dielectric spectroscopy; differential scanning calorimetry.

1. Introduction

Liquid crystals (LC) are interesting materials as their molecules are relatively free to move while maintaining a long-range orientational order in phases known as mesophases because they are considered intermediates between the ordered solid crystalline phases and the disordered isotropic liquid states [1]. Among them, LC dimers have been the focus of many research activity not only at the fundamental level, but also by their potential experimental applications [2, 3].

In these materials two semi-rigid units are linked by a flexible spacer such as an alquil chain. The most widely synthesized dimers are those with calamitic mesogenic rigid groups connected by ether or methylene linkages [4]. Depending on the nature of the involved units we can distinguish between symmetric (both units are identical) and non-symmetric LC dimers with different rigid units in the molecule. The resulting material generally shows unusual properties as enhanced

*Corresponding author. Email: jose.antonio.diego@upc.edu

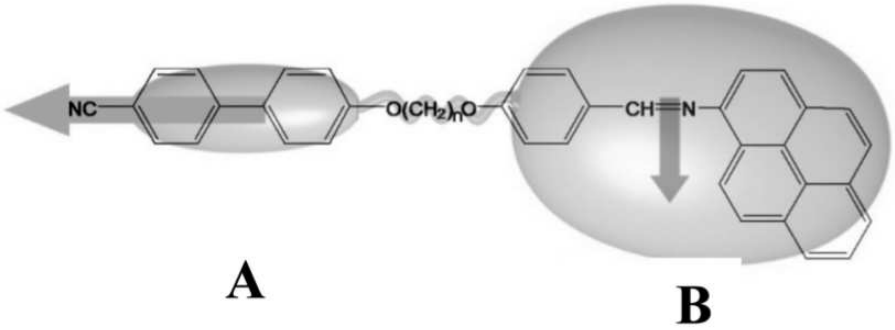

Figure 1. Scheme of the CBOnO.Py molecule.

electro-optical properties and anysotropy, additional molecular motions, new mesophases (alternating and modulated smectic mesophases [2, 3, 5–9], the recently discovered twist-bend nematic mesophase [10–19], ...). Such properties may conform the base of new electro-optical devices as displays, wave-guides or lasers, that take advantage of the enhanced molecular orientations and/or arrangements in the material [1, 4].

Interestingly, the length, parity and nature of the flexible spacer chain strongly affects the properties of the material. Odd-even effect has also been observed in transition temperatures and entropy changes [4, 5], so studies on these properties should be restricted to odd or even members of a given series. This is the case of the non-symmetric LC dimers studied in the present work, that belongs to the series α-(4-cyanobiphenyl-4´-oxy)-ω-(1-pyreniminebenzylidene-4´-oxy) alkanes (CBOnO.Py) with $n = 3$, 5, 7 and 9 shown in figure 1.

These compounds exhibit an important dipole moment along its long axis, associated with the nitrile group A (horizontal arrow in figure 1), while an smaller and mainly transverse dipole moment appears associated with the imine group B (drawn in figure 1 as a perpendicular arrow). One interesting property about this family of dimers arises from the fact that different LC mesophases can be obtained depending on the length of the spacer chain. CBOnO.Py with n=3 and n=11 are nematogenic while n=5,7,9 are smectogenic.

A previous work by Stocchero et al [20] was very useful in interpreting dielectric and structural relaxations in CBOnO.Py series [8, 21, 22]. Three dielectric relaxations were observed at temperatures above the glass transition by Broadband Dielectric Spectroscopy (BDS). The low frequency relaxation was associated to the flip-flop motion of the pyrene group (m_{1L} in [22]), which immediately forces the cyanobiphenil unit to reorient and, therefore, can be detected dielectrically. The intermediate frequency relaxation was attributed to the flip-flop reorientation of the cyanobiphenil unit (m_{1H} in [22]), and both relaxations were present only when the molecules showed a homeotropic-like orientation parallel to the electric field. The dielectric spectrum, when molecules are orientated perpendicular to the probe electric field, is dominated by a high frequency relaxation process (m_2 in [22]). This relaxation was associated to the superposition of the precessional motions of the semirigid units and the rotation of the molecule around its long axis, as described by the Nordio-Rigatti-Segre theory [23].

It should be stressed as a noteworthy result for CBO11O.Py that as the glass transition temperature is approached, the above mentioned three relaxations do not converge at a unique glass transition temperature [21]. Results showed that m_2 and m_{1H} relaxations become indistiguishable at the glass transition temperature $T_{g1} = 302$ K, whereas m_{1L} glass transition is observed approximately 7 K above. Detection of these two glass transition temperatures was performed by several techniques: Broadband Dielectric Spectroscopy (BDS), Thermally Stimulated Depolarization Currents (TSDC) and calorimetry, however TSDC turned out to be the most sensitive among them. TSDC is a valuable technique to study dielectric relaxations, as Broadband Dielectric spectroscopy, but at the very-low frequency range (10^{-3} to 10^{-4} Hz) [24] with much greater sensitivity

Table 1. Some thermal parameters used for each material in the TSDC experiments.

n	T_I (K)	T_0 (K)	T_d (K)	t_d (min)	T_f (K)
3	–	338	288	15	338
5	443	315	278	15	323
7	448	330	278	15	330
9	443	315	273	15	327

in studying the glass transition [25–28].

In this work, we have analyzed by means of TSDC and BDS techniques, the relaxation modes of odd members ($n = 3$ to 9) of the non-symmetric liquid crystal dimers α-(4-cyanobiphenyl-4´-oxy)-ω-(1-pyreminebenzylidene-4´-oxy) alkanes or CBOnO.Py in the supercooled mesophase and the glassy state. The main purpose is to study the evolution of the aforementioned molecular motions and to determine the role that the length of the flexible spacer plays in their kinetics and in the complexity of the relaxations. The presence or not of unfolded glass transitions in these materials will also be examined. For sake of comparison, results already published corresponding to the longuer homologue LC dimer of the series ($n = 11$) will be considered.

The paper is organized as follows: in section 2 we explain the experimental techniques, including a detailed description of TSDC, in section 3 the results are presented and discussed and, finally, in section 4 we arrive to the main conclusions

2. Experimental

2.1 *Preparation of the materials in the nematic or smectic A glassy states.*

Pure CBOnO.Py ($n = 3$, 5, 7, 9) compounds were synthesized and purified according to the work of Attard et al. [29]. In order to study the glass transition by TSDC, prior to the measurements each material was obtained in the nematic or smectic A glassy state following a convenient thermal treatment. In the case of CBO3O.Py, the nematic-isotropic (N-I) transition occurs around 388 K [22] and the material does not crystallize in the temperature range between 300 and 400 K, where the glass transition is located ($T_g = 323.3$ K). So no special thermal treatment is necessary for this LC dimer.

The rest of compounds studied in this paper ($n = 5$, 7, 9) exhibit monotropic SmA mesophases and the glassy state can be achieved at relatively low cooling rates of 5 K/min ($n = 5$), 1 K/min ($n = 7$) and 2 K/min ($n = 9$). However, both LC ($n = 5$, 7) show a hot crystallization (SmA $\Rightarrow$ Cr) on heating, a fact that also occurs in an isothermal treatment, some degrees above T_g. For CBO7O.Py this crystallization takes place once the SmA to N phase transition occurs.

In TSDC experiments and according to the thermal behaviours described above, each sample was heated to the isotropic phase at T_I and cooled down to T_0 at a rate of 40 K/min. Special care was taken in selecting the initial temperature of the TSDC measurement (T_0) that must yield above T_g but below the crystallization temperature. Values of T_I and T_0 chosen in each case are listed in table 1.

Microscopic observations under polarized light were performed to confirm the amorphous state and the alignment of the samples prepared by this procedure. Figure 2 shows the typical nematic domains of the amorphous phase obtained for CBO7O.Py after the thermal treatment. Similar amorphous textures where obtained for the other compounds investigated in at least more than 95 % of the sample.

2.2 *TSDC experiments*

In the Thermally Stimulated Depolarization Currents technique, charges in the material are activated by a poling field at a temperature where they can be oriented, and then frozen by cooling

Figure 2. Optical texture by POM for CBO7O.Py after the TSDC thermal treatment. Typical nematic domains within the amorphous material can be appreciated together with some scarce crystalline nuclei.

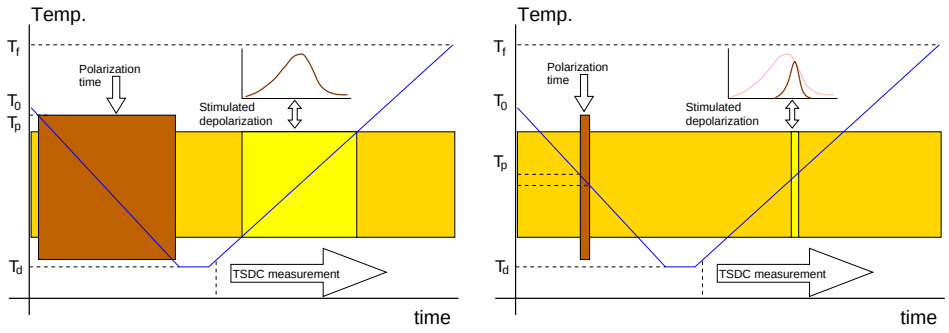

(a) Complete poling measurement (b) NIW partial polarization measurement.

Figure 3. Schematic representation of a TSDC experiment.

down the sample. The sample is then depolarized by heating at a constant rate while the resulting current intensity is recorded as a function of temperature. The polarization and depolarization processes in TSDC have been widely described in the literature [30, 31]. The intensity measured by this technique reveals the existence of different kinds of charge relaxations, such as the dipolar α relaxation which is the dielectric manifestation of the glass transition in polar materials. One interesting feature of TSDC is its ability to resolve a distributed process into more elementary contributions [32, 33]. An elementary spectrum can be described more accurately in terms of a single relaxation time and can be thus better studied according to existing models.

Figure 3 shows a typical poling-temperature scheme in a TSDC experiment. In a conventional measurement the material is poled at high temperature and cooled down below the relaxation temperature range without removing the electric field. In this way, all the polarization is frozen in the material that becomes an 'electret' [24, 31]. The electret is then heated at a constant rate and a depolarization current is obtained when the relaxation mechanism is activated (Figure 3.a). If the electric field is 'on' only in a very small temperature range during the cooling ramp (non-isothermal window (NIW) partial poling method, Figure 3.b), only polarization associated to the mobility recovered at that temperature will be frozen [25, 34, 35]. A complex relaxation, as that commonly related to the glass transition, can be resolved by this poling procedure into more elementary spectra because in the subsequent heating ramp only the contribution of this small fraction of the relaxation will be detected. The whole relaxation results then from the superposition of the elementary contributions obtained at different polarization temperatures in the so called 'Relaxation Map Analysis' study (RMA) [26, 36].

Samples for TSDC experiments consisted in 5 μm thick commercial Linkam cells filled with liquid crystals by capillarity with 1 cm^2 ITO coated electrodes in the inner side of the cell. Thermal stimulated depolarization currents were performed by means of a non-commercial experimental setup controlled with an Eurotherm 904P temperature programmer. Temperature was measured with an accuracy of 0.1 K using a PT-100 thermoresistance located near the sample, and current intensity during depolarization was recorded with a Keythley 6512 electrometer. Both sample alignments, parallel and perpendicular to the probe electric field, were selected for TSDC using polarization fields ranging from 1 MV/m to 9.6 MV/m.

At the beginning of each experiment, the sample (in the glassy state) is at a temperature T_0. From this temperature, the sample is cooled at a constant cooling rate of 2.5 K/min down to T_d. During the cooling ramp the electric field is switched 'on' at T_p and removed at a temperature $T_p - \Delta T_p$. The sample, now an electret, remains at T_d for a deposit time t_d and then it is heated at a constant rate of 2.5 K/min up to T_f while the depolarization current is measured. In Table 1 are listed the values of T_0, T_d, t_d and T_f used for each material in all the experiments. Additional details of the experimental technique can be found elsewhere [34, 37, 38].

2.3 *BDS measurements*

Experimental measurements of the real and imaginary parts of the dielectric permitivity were carried out by means of an Alpha impedance analyzer from Novocontrol from 10^{-3} Hz to 10^6 Hz and temperatures between 300 K and 400 K. Samples consisted on 5 mm diameter plane capacitors prepared between gold-plated brass electrodes with 50 μm thick silica spacers. Temperature was controlled by means of a System Quatro from Novocontro with stabilization at different temperatures with a precision of the order of 20 mK. Additional details of the experimental technique can be found elsewhere [39, 40].

2.4 *MDSC measurements*

Heat capacity measurements were obtained by Modulated Differential Scanning Calorimetry (MDSC) with a TA Instruments Q2000 calorimeter. The MDSC technique, in addition to specific heat data, simultaneously provides phase shift data (Φ) that allow determining the coexistence region in weakly first-order phase transitions. Experiments were performed on $3 - 7$ mg samples sealed in aluminium pans on cooling from the I phase down to the mesophase and next on heating; the temperature rate on cooling was 2 K/min and on heating were of 1, 2.5 and 5 K/min, with a modulation temperature amplitude of ± 0.5 K and a period of 60 s. Extensive details about this technique can be found elsewhere [39, 40].

2.5 *Polarized optical microscopic observations*

Samples for POM observations where prepared in Linkam cells filled with the LC dimmers by capillarity. The cell is placed in a Linkam THMSG-600 hot stage and temperature is controlled via a Linkam TMS-94 temperature controller. Optical textures were recorded with a Kyowa polarizing microscope at different stages of the thermal treatment.

3. Results and discussion

Before coming to the presentation and discussion of the central experiments object of this work, this is, the TSDC measurements, we would like to begin with the description of the broadband dielectric spectroscopy studies (BDS) (section 3.1). This is motivated by the fact that BDS is much more established in the liquid crystals community and, together with some recent results from the

authors, will allow us to identify the different molecular motions that are responsible of the glass transitions. After stating this basis, we will proceed with the TSDC measurements, first following a "complete poling" scheme with several poling conditions in order to detect and characterize the glass transition/s of each LC dimer (section 3.2) and later performing the RMA study (see section 2 for details) of all the detected transitions in each LC dimer (section 3.3). The TSDC data will be then fitted to some phenomenological models (section 3.4) and, finally, we will make a comparison of calorimetric data obtained from MDSC measurements and from a model that makes use of the TSDC results (section 3.5).

3.1 *Broadband dielectric spectroscopy*

The dielectric behaviour of these LC dimers far from the glass transition has already been published [8, 22]. Complex dielectric permittivity data were fitted to the Havriliak-Negami empirical function:

$$\epsilon(\omega) = \sum_k \frac{\Delta\epsilon_k}{[1 + (i\omega\tau_k)^{\alpha_k}]^{\beta_k}} + \epsilon_\infty - i\frac{\sigma_{\mathrm{DC}}}{\omega\epsilon_0} \tag{1}$$

where k accounts for the relaxation modes present in the phase; $\Delta\epsilon_k$ and τ_k are the dielectric strength and the relaxation time related to the frequency of maximum dielectric loss, respectively; α_k and β_k are parameters that describe the shape (width and symmetry) of the relaxation spectra; ϵ_∞ is the dielectric permittivity at high frequencies (but lower than those corresponding to atomic and electronic resonance phenomena); and σ_{DC} is the electric conductivity. With respect to the α_k and β_k parameters, both are equal to 1 in the simplest (Debye) model. If the relaxation is more complex, the shape of the peaks may get broader ($\alpha_k < 1$, Cole-Cole relaxation type) and/or asymmetric ($\beta_k \neq 1$, Cole-Davidson relaxation type).

For frequencies above 15 Hz all the investigated CBOnO.Py dimers show three separated relaxations. Depending on the DC bias applied, the sample adopts a mixed alignment or an alignment parallel to the probing electric field (homeotropic alignment). In parallel alignment two relaxations, both Debye-like, were detected, (m_{1L} and m_{1H}), and in mixed aligned samples a higher frequency relaxation (m_2), Cole-Cole type, was observed. These results can be explained in the framework of Stocchero's theoretical model for the dielectric behavior of non-symmetric LC dimers [20]. The m_{1L} and m_{1H} relaxations are observed when the molecules show a homeotropic alignment, parallel to the electric field. However, the m_2 relaxation is observed when the molecules are perpendicular to the electric field (planar alignment). In a homeotropic-like alignment, as the temperature decreases, the strength of m_{1L} increases up to a saturated value, while the strength of m_{1H} goes down to values close to zero, which claims how the dielectric strengths of both m_{1L} and m_{1H} relaxation modes are highly coupled. The high frequency mode, m_2, has a small strength in homeotropic alignment.

For dielectric relaxations, a glass transition (denoted as dynamic glass transition) is obtained when the characteristic relaxation time, τ, of the associated relaxation mode reaches 100 s. Measurements in the low frequency range, when approaching the glass transition, have been carried out in CBO3O.Py, CBO7O.Py and CBO9O.Py (measurements in CBO5O.Py were not possible as a consequence of the irreversible crystallization of the material during the experiment).

As it was observed for CBO11O.Py ([21]), BDS measurements carried out in this frequency range suggest that m_2 and m_{1H} tend to merge at low frequencies while m_{1L} seems to remain always as a separated relaxation for CBO7O.Py and CBO9O.Py. In CBO3O.Py also the lowest frequency mode seems to merge with the other two at the glass transition, but the experimental data are not as confident as in the other dimers to make such an assertion. As an example, Figure 4 shows the relaxation time of the dielectric modes for CBO9O.Py in an Arrhenius plot ($\log_{10}\tau$ vs $1000/T$). It is easy to observe how the maxima corresponding to m_{1H} and m_2 are indistinguishable at times above 3 s.

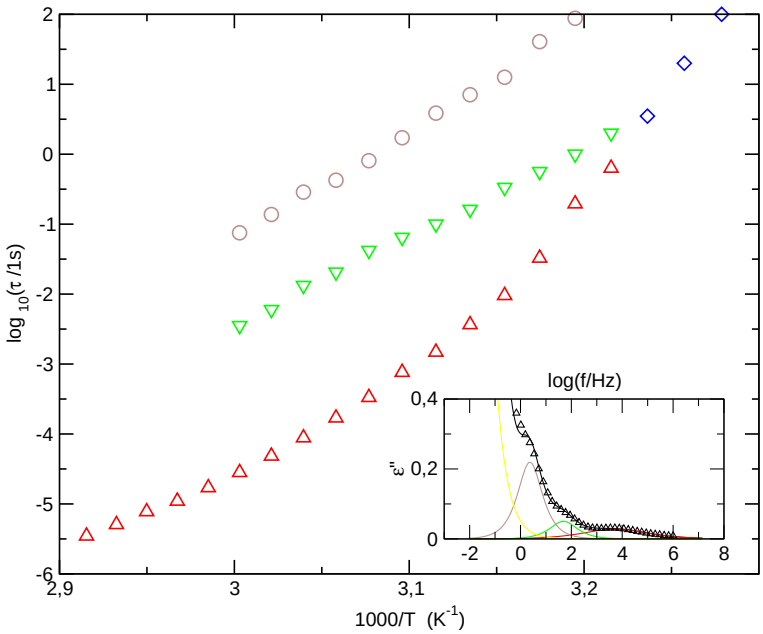

Figure 4. Relaxation times at the frequency of maximum dielectric loss for m_{1L} (black), m_{1H} (red) m_2 (green) and m_2+m_{1H} (blue). The values correspond to the CB9O.Py dimer. The inset shows the frequency dependence of the imaginary part of the permittivity at 327 K. The lines represent deconvolution into elementary modes according to the Havriliak-Negami equation.

Table 2. Poling temperatures used in the complete poling study for each LC dimer.

LC dimer	n=3	n=5	n=7	n=9
T_p (K)	330	315	319	314
ΔT_p (K)	23	23	27	29

The low frequency relaxation mode (m_{1L}) can be associated to the flip-flop motion of the pyrene group, which immediately forces the cyanobiphenyl unit to reorient and, therefore, can be detected dielectrically. The intermediate frequency mode (m_{1H}) can be attributed to the flip-flop reorientation of the cyanobiphenyl unit and the high frequency one (m_2) is due to the precession of the same cyanobiphenyl group around the molecular nematic director [15]. These two modes merge when arriving to the glass transition, which means that each rigid unit in the dimer is responsible of one of the two glass transitions. Steric interactions in the nematic or smetic A environment in the case of the pyrene group are stronger than in the case of the cyanobiphenyl unit, fact that explains the difference in temperatures of both relaxations at these low temperatures ($T_g(Py) > T_g(CB)$).

3.2 *Complete poling study*

To characterize the glass transition of these materials a 'complete poling scheme' was carried out, in which ΔT_p spans the temperature range in which the relaxation associated to the glass transition can be activated. The values of T_p and ΔT_p used for each investigated compounds are listed in Table 2.

Different poling fields were analyzed: from a relatively low field (1 MV/m) in which a mixed orientation of the molecules is present, to a quite high poling field of 8 MV/m for which most of the molecules align parallel to the applied field (homeotropic alignment). The TSDC results clearly show two differentiated behaviours: on one side that for CB3O.Py with the shorter flexible spacer and on the other side, the rest of the LC dimers of the series. The TSDC spectra for the latter ($n = 5$, 7 and 9) show, at low poling fields, the presence of a double discharge peak, as was observed previously for CBO11O.Py [21]. The temperature difference ΔT between the maxima of these peaks

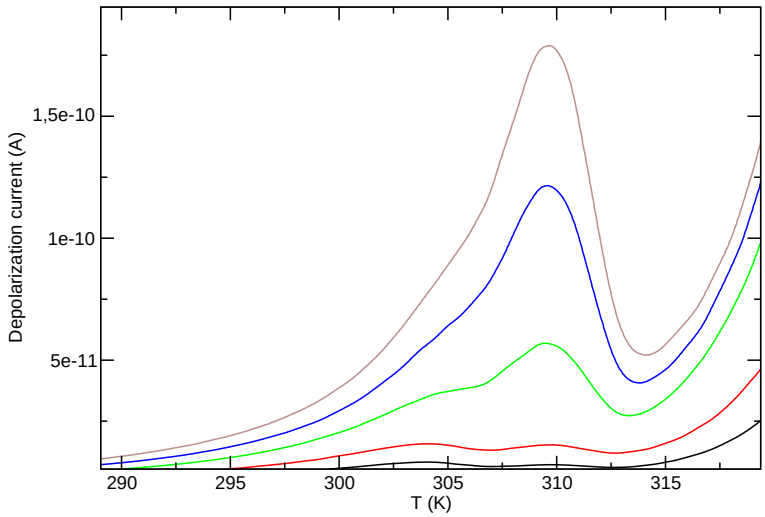

Figure 5. Complete poling TSDC spectra obtained with CBO7O.Py at different poling fields: 1 MV/m (black), 2 MV/m (red), 4 MV/m (green), 6 MV/m (blue), and 8 MV/m (brown).

slightly increases for compounds of the series as the spacer is longer. When increasing the electric field the high temperature peak intensity is observed to increase being clearly predominant. Figure 5 shows, as an example, the TSDC spectra obtained for CBO7O.Py under poling fields of 1, 2, 4, 6 and 8 MV/m. It can be clearly seen the presence of two discharge peaks, the first one at 304.0 K and the other at 309.5 K which becomes predominant for high poling fields. Since TSDC measurements are equivalent to BDS measurements at very low frequencies ($< 10^{-3}$) [24], this behavior confirms the existence of two glass transitions. Indeed, TSDC results show two separated discharge peaks: one corresponding to the molecular motions represented by m_2 and m_{1H} relaxation modes, both indistinguishable at low enough temperatures and the other compatible with the m_{1L} relaxation mode. As was already stated for CBO11O.Py in a previous work ([21]), the high temperature discharge peak observed in these measurements must be associated to the dielectric relaxation mode m_{1L} (due to motions of the pyrene group), which is present when the molecules show a homeotropic alignment. The low temperature relaxation can be attributed to a sum of both the m_{1H} and the m_2 modes, which account for the motions of the cyanobiphenyl unit [21].

It is thus concluded that LC dimers CBOnO.Py for $n = 5$, 7 and 9 show two differentiated glass transition temperatures which are separated approximately 4.5 K for $n = 5$ and 5.5 K for $n = 7$ and $n = 9$. These results are in good agreement with the previous work of CBO11O.Py, which showed a double glass transition in which the difference between both glass transition temperatures is 7 K [21]. It should be stressed that such a temperature separation between both glass transitions is favored and seems to be increased with the flexible alquil chain spacer (n), a fact coherent with a decoupling and differentiation of those motions related to each terminal unit. Figure 6 shows this evolution in the TSDC scans obtained for all the LC dimers of the series with $n = 5$ up to 9 at 2 MV/m poling field. We can also see that the m_{1L} relative intensity in each scan increases with the length of the spacer as due to the increased homeotropic-like alignment of the LC dimer because it gains flexibility.

A special poling scheme has been carried out in order to obtain further insight into the origin of each discharge peak. In this poling procedure, the sample is heated up to the isotropic phase and then it is cooled down to the mesophase (nematic or smectic A) with a high electric field applied. By this way a high homeotropic-like molecular alignment of the material is obtained. Once the high homeotropic-like oriented phase takes place, the sample is poled following the complete poling scheme discussed above and the TSDC discharge is measured.

Figure 7 shows, for CBO5O.Py, the complete poling spectra obtained in mixed (red curve) and homeotropic-like (black curve) alignments. It is clear that the low temperature peak ($m_2 + m_{1H}$) is

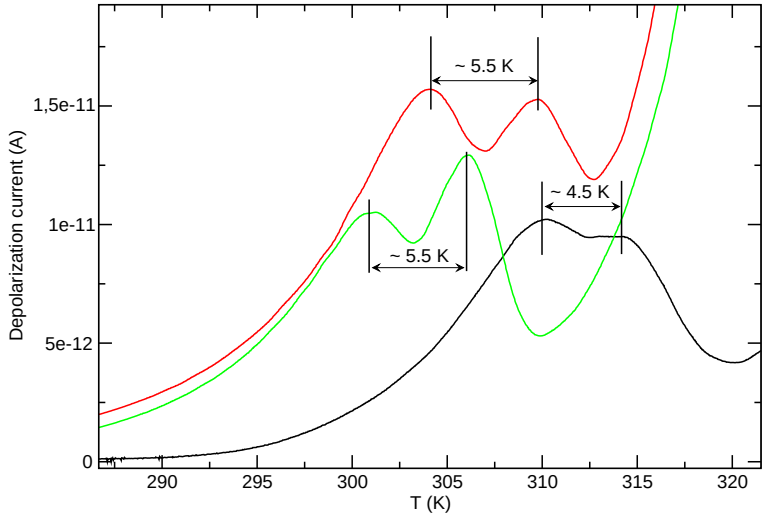

Figure 6. Complete poling TSDC spectra obtained with CBO5O.Py (black), CBO7O.Py (red) and CBO9O.Py (green) at 2 MV/m.

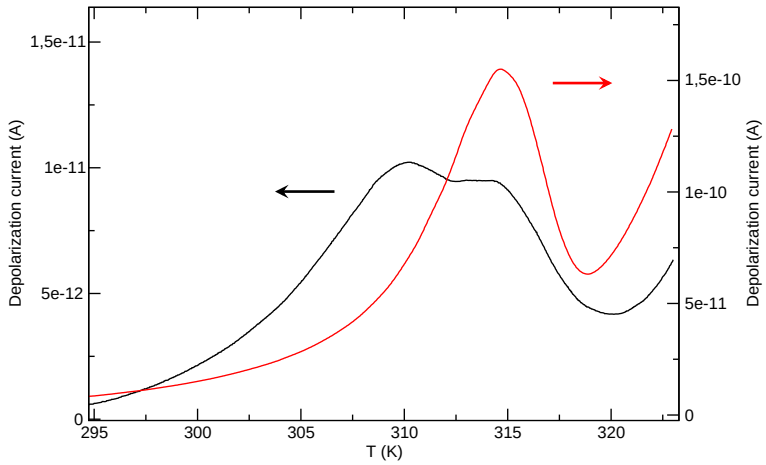

Figure 7. Complete poling TSDC spectra obtained with an CBO5O.Py sample with high homeotropic-like orientation and with mixed orientation. (Red: sample quenched from the isotropic phase, under the influence of a high electric field (8 MV/m), down to the nematic phase and then poled at 8 MV/m. Black: mixed oriented sample poled at 2 MV/m).

almost undetectable in the homeotropic-like oriented sample, which is coherentt with Stocchero's model [20]. When approaching the glass transition, m_{1H} becomes weaker and tends to merge with m_2, being impossible to be observed in homeotropic-like alignment when high poling fields are applied.

Textures from polarized optical microscopy (POM) of the material at different stages during the TSDC measurement also agree with the above interpretation of the peaks. Figure 8 shows optical textures in polarized light obtained for CBO9O.Py. At the beginning of the scan, at low poling field (1.5 MV/m, black curve) the sample shows a mixed alignment, whereas at higher poling field (8 MV/m, red curve) the sample shows a more homeotropic-like alignment.

TSDC scans obtained in CBO3O.Py do not show a double peak at any poling field, however some significant evolution is observed when the poling field is increased as shown in Figure 9. For poling fields below 8 MV/m (curves a, b, c of Figure 9) a mixed alignment is present in the sample and a unique discharge peak is observed at about 317.5 K. However, at high enough poling fields (curve d) the discharge peak shifts approximately 1 K at higher temperatures and remains for any poling field (see curves e, f and g). If the sample is heated up to the isotropic state and cooled down, the former discharge peak (at about 317.5 K) reappears for low poling fields (only the curve for

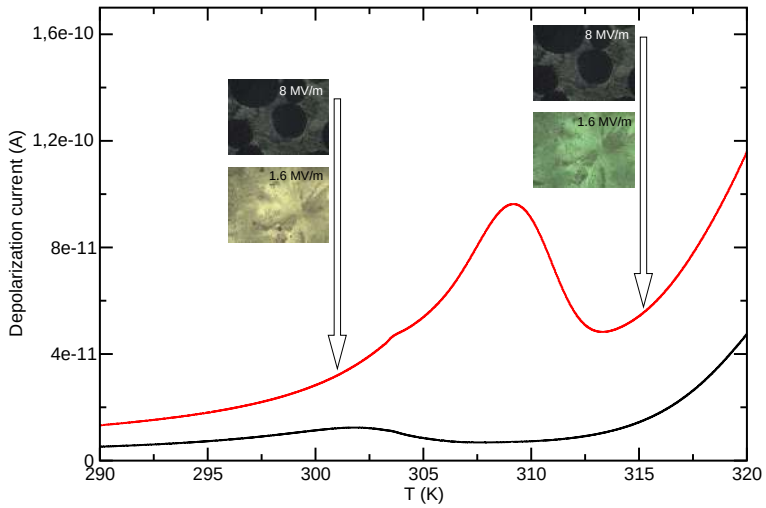

Figure 8. Textures obtained from polarized optical microscopy in CBO9O.Py during a complete poling TSDC spectra obtained with different poling fiel

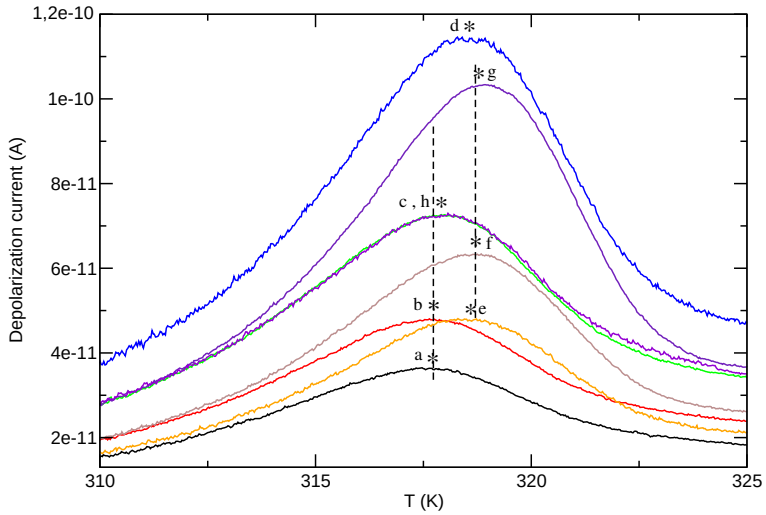

Figure 9. Complete poling TSDC spectra obtained with an CBO3O.Py sample at different thermal and electrical histories: (a) quenched from the isotropic phase and poled at 3 MV/m, (b) subsequent poling of the sample at 4 MV/m, (c) subsequent poling of the sample at 6 MV/m, (d) subsequent poling of the sample at 8 MV/m, (e) subsequent poling of the sample at 3 MV/m again, (f) subsequent poling of the sample at 4 MV/m again, (g) subsequent poling of the sample at 6 MV/m again, (e) quenched again from the isotropic phase and poled at 6 MV/m.

6 MV/m is shown, curve h) and the whole process can be reproduced. This fact could be explained assuming that the two discharge peaks are very close to each other because the spacer is short and the rigid units are highly coupled. When the sample is cooled down from the isotropic state and low poling fields are applied, the mixed alignment is present. So, the observed discharge peak accounts for all molecular motions. However, when the sample is subjected to a high electric field, almost a complete homeotropic-like molecular alignment is achieved and only the high temperature relaxation takes place. Heating the sample up to te isotropic state and cooling it down back, the mixed alignment reappears.

3.3 *RMA study of the $m_2 + m_{1H}$ and m_{1L} relaxations*

We can take advantage of the ability of the RMA-TSDC technique to resolve a complex discharge peak, as the one related to the glass transition for the LC dimers, into debye-like components.

Table 3. Poling temperatures used in the RMA study for each LC dimer. T_p ranges from T_pi to T_pf in 1K steps with $\Delta Tp = 1K$ window width.

n	3	5	7	9
T_pi (K)	55	42	46	41
T_pf (K)	35	20	16	14

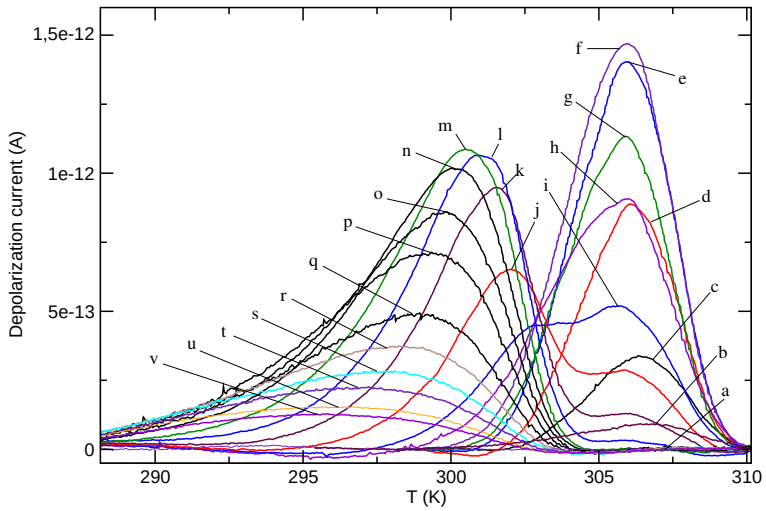

Figure 10. Experimental spectra of CBO9O.Py obtained by RMA-TSDC at different T_p, from 309 K to 288 K in 1 K increment steps (curve a: $T_p = 309$ K, curve b: $T_p = 308$ K, curve c: $T_p = 307$ K, ..., curve v: $T_p = 288$ K).

For this purpose a poling scheme with $\Delta T_p = 1$ K and different poling fields between 1 MV/m and 8 MV/m has been carried out. In Table 3 the values of T_p used for each compound in these experiments are listed.

Figure 10 shows the typical RMA spectra obtained for CBO9O.Py with a poling field of 2 MV/m. For high poling temperatures above 309 K (curve a) no discharge peak is observed because the material is way above the glassy state when the electric field is removed and, thus, it depolarizes almost instantaneously during the rest of the cooling ramp. For poling temperatures of 308 K–307 K (curves b, c) the emergence of a discharge peak is observed around 306 K. This fact occurs because the poling field is now applied at the upper limit of the glass transition temperature range, and some molecular motions get restricted at this temperature. As a result, some polarization remains frozen in the material and consequently a discharge curve appears during the subsequent heating ramp.

A maximum in the discharge peak of 306 K is observed for a poling temperature of 305 K (curve f), also called the 'optimum poling temperature' (T_{po}). This temperature is directly related to the glass transition temperature of the material [41]. As T_p decreases, this high temperature peak disappears because the related molecular motions are already restricted when the electric field is applied, but a new low temperature discharge peak emerges around 302 K (curve i). These measurements confirm, thus, the presence of two glass transitions in the material associated to the $m_2 + m_{1H}$ and to the m_{1L} molecular motions. We can see as well that the poling temperatures where $m_2 + m_{1H}$ peak is detectable are broader than those for m_{1L} peak. The maximum of the low temperature peak is obtained approximately at 301 K for $T_p = 297$ K (curve m), and it can be appreciated for poling temperatures as low as 288 K as a broad discharge current around 297 K (curve v). This result indicates that the peak related to the $m_2 + m_{1H}$ mode is more distributed than that of m_{1L}.

Measurements performed at different poling fields and with $n = 7$ and $n = 5$ LC dimers show

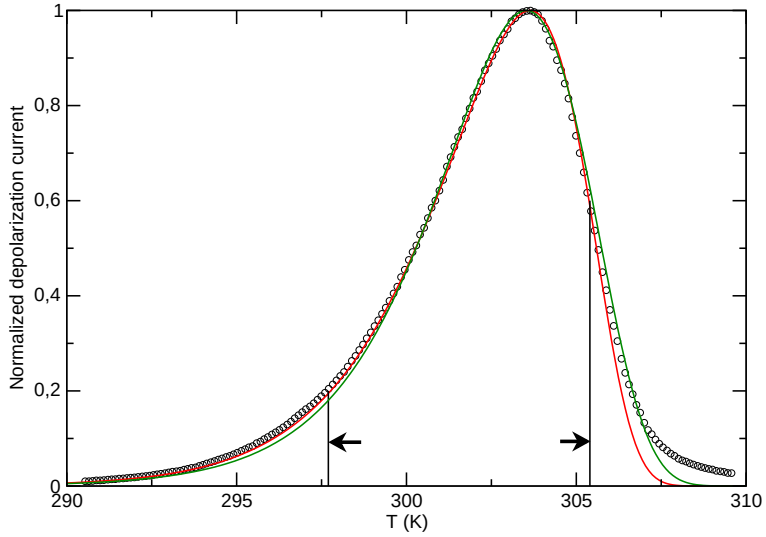

Figure 11. Comparison of the Arrhenius model (green line) and the TNM model (red line) fits to experimental data (circles) obtained with CBO7O.Py by RMA-TSDC at the optimal polarization temperature of the low temperature relaxation (T_p = 300 K, $E_p = 4$ MV/m). Arrows indicate the fitted range of temperatures.

similar results, with two discharge peaks for $n = 9$ ($T(m_2 + m_{1H}) = 300.4$ K, $T(m_{1L}) = 305.9$ K), $n = 7$ ($T(m_2 + m_{1H}) = 303.5$ K, $T(m_{1L}) = 309.2$ K) and $n = 5$ ($T(m_2 + m_{1H}) = 308.5$ K, $T(m_{1L}) = 313.0$ K). In the case of the $n = 3$ dimer, with the shorter flexible spacer of the n-methylene groups, only one discharge peak is observed that appears at 319.6 K when poling at the T_{po}. This behaviour suggests again that both relaxations are highly coupled and occur simultaneously in these experiments, as we have already discussed.

3.4 *Modeling of the relaxation time*

Discharge curves obtained in the RMA-TSDC measurements can resolve a complex discharge peak into more elementary contributions that can be, therefore, better described in terms of a simple relaxation time. If the relaxation mechanism is a first order kinetic one, the calculated depolarization current density can be obtained according to the equation:

$$J(T) = \frac{P_0}{\tau(T)} \exp\left[-\frac{1}{\beta}\int_{T_0}^{T}\frac{dT}{\tau(T)}\right] \tag{2}$$

were P_0 is the initial polarization, $\tau(T)$ is the relaxation time, T_0 is the initial temperature and β is the heating rate. Several empirical models of $\tau(T)$ can be checked in this way by fitting TSDC data according to equation 2. A more detailed explanation of this procedure can be found elsewhere [25, 26].

We have checked the obtained TSDC data against two phenomenological models for $\tau(T)$ usually applied to calorimetric and dilatometric measurements: the Arrhenius model and the Tool-Narayanaswamy-Moynihan model (TNM).

Figure 11 shows a comparison of the fitted curves obtained with each model for the low temperature peak ($m_2 + m_{1H}$) of CBO7O.Py polarized at the T_{po} ($T_p = 300$ K, $E_p = 4$ MV/m) according to the calculated parameters listed in Tables 4 and 5. It can be observed that the best results for this peak are obtained with the TNM model (red curve in Figure 11) in which $\tau(T)$ obey the equation:

$$\tau(T, T_f) = \tau_0 \exp\left(\frac{xE}{RT} + \frac{(1-x)E}{RT_f}\right) \tag{3}$$

Table 4. Some representative parameters obtained from the mathematical fit to the TNM model of the RMA-TSDC curves obtained at the T_po of the low temperature relaxation ($m_2 + m_{1H}$) for each LC-dimer (values for $n = 11$ from [21]).

n	τ_0 (s)	E_a (eV)	x
5	4×10^{-57}	3.56	0.92
7	2×10^{-67}	4.11	0.83
9	1×10^{-71}	4.32	0.80
11	4×10^{-70}	4.25	0.72

Table 5. Some representative parameters obtained from the mathematical fit to the Arrhenius model of the RMA-TSDC curves obtained at the T_{po} of the high temperature relaxation (m_{1L}) (values for n=11 from [21]).

n	τ_0 (s)	Ea (eV)
7	9×10^{-60}	3.73
9	8×10^{-73}	4.48
11	9×10^{-66}	4.11

where τ_0 is the pre-exponential factor, E_a is the activation energy, T_f is the fictive temperature and x ($0 <= x <= 1$) is the non-linearity parameter. The fictive temperature (T_f) and the non-linearity parameter (x) are introduced to take into account memory effects in the structural conformation of the system. The fictive temperature of a non-equilibrium system can be understood as the temperature of an equilibrium system with the same structural conformation.

The evolution of T_f with the thermal history of the sample is modeled assuming an ideal-viscous return to equilibrium, that also depends on $\tau(T)$ according to equation:

$$\frac{dT_f}{dt} = - \frac{T_f - T}{\tau(T, T_f)} \tag{4}$$

Equations 3 and 4 are coupled and have been resolved using numerical methods explained elsewhere [25].

Unlike the low temperature peak ($m_2 + m_{1H}$), the best numerical fit of TSDC data for the high temperature peak (m_{1L}) is obtained when $x = 1$, the Arrhenius model. Figure 12 shows the curve obtained for the m_{1L} peak of CBO7O.Py polarized at its T_{po} ($T_p = 308$ K, $E_p = 4$ MV/m) according to the fitted values listed in Table 5. In this case the discharge peak is more symmetric and less distributed.

These results indicate that the low temperature discharge peak ($m_2 + m_{1H}$) is much more distributed than the high temperature one (m_{1L}), which is coherent with the fact that the former is the result of several different mechanisms. Also, as most of the material is still in the glassy state at this temperature, the partial hindering of molecular motions may be another cause of the non-linearity nature of the relaxation.

Similar behaviors are obtained for the $m_2 + m_{1H}$ and m_{1L} discharge peaks of each LC dimer of the series ($n = 5$, 7 and 9). In all these cases the best results are obtained with the Tool-Narayanaswamy-Moynihan model for the low temperature peak and with the Arrhenius model for the high temperature peak.

In Tables 4 and 5 are listed the kinetic parameters obtained by numerical fit of the TSDC

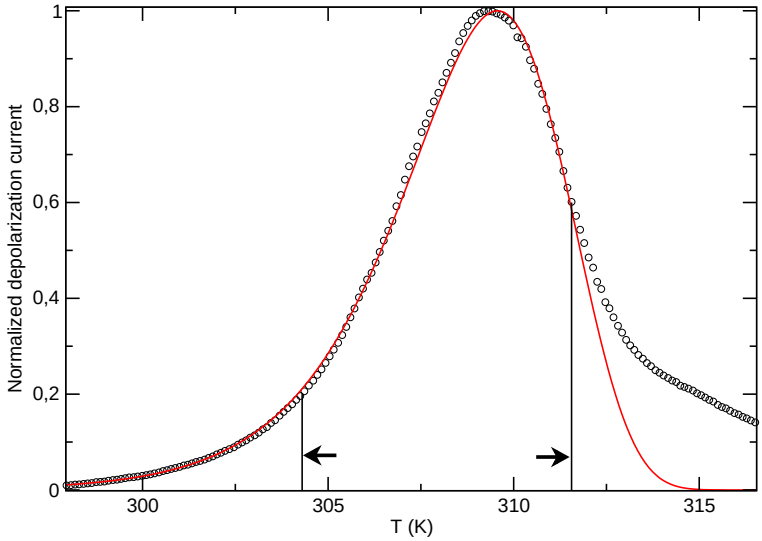

Figure 12. Arrhenius fit (red line) of experimental data (circles) obtained with CBO7O.Py by RMA-TSDC at the optimal polarization temperature of the high temperature relaxation ($T_p = 308$ K, $E_p = 4$ MV/m). Arrows indicate the fitted range of temperatures.

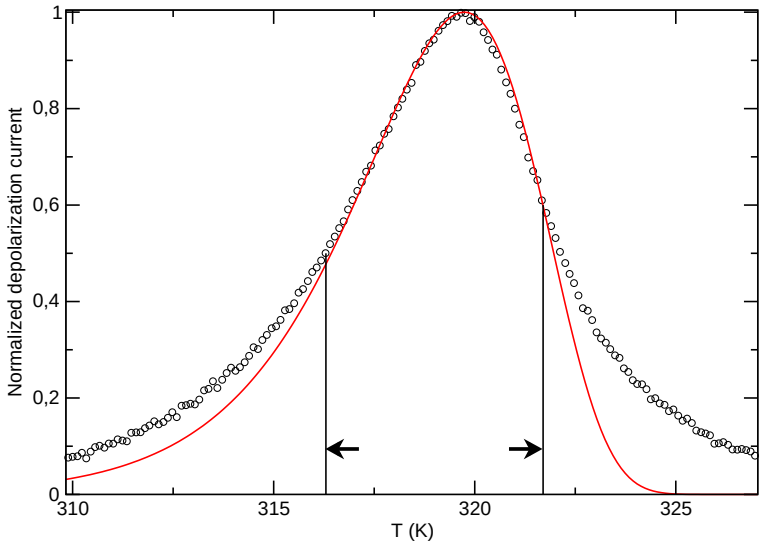

Figure 13. TNM fit (red line) of experimental data (circles) obtained with CBO3O.Py by RMA-TSDC at the optimal polarization temperature of the relaxation ($T_p = 320$ K, $E_p = 3$ MV/m). Arrows indicate the fitted range of temperatures.

curves for the main contribution of each peak, that corresponds to the T_{po}. Previous results for CBO11O.Py [21] are also reproduced in order to make comparison possible.

Aside from the increased complexity of the $m_2 + m_{1H}$ discharge peak with respect to the m_{1L} peak in all the dimers investigated, the non-linearity parameter (x) obtained for the $m_2 + m_{1H}$ peak also decreases as the flexible spacer length increases. This result indicates that complexity also increases with the length of the spacer. As a general trend, we can appreciate as well in both relaxations a slight increase in the activation energy with n, at the time the pre-exponential factor decreases gradually.

In the case of CBO3O.Py neither the TNM nor the Arrhenius model can reproduce satisfactorily the obtained RMA-TSDC spectra. As it can be seen in figure 13, the discharge curves for this dimer show a single peak with a broad left and right tails, that none of the aforementioned models can deal with. We must remember however that in this case the resulting discharge peak comes from the superposition of several molecular motions, that take place simultaneously. Best results are

obtained with the TNM model with $x = 0.98$, very close to the Arrhenius model. Figure 13 shows the fitted curve obtained for the main mode of the RMA spectra (T_p = 320 K, E_p = 3 MV/m) with $\tau_0 = 6 \times 10^{-61} s$ and $E_a = 3.93eV$.

3.5 *Simulation of calorimetric response*

An interesting feature of the modeling that has been carried out is the possibility of reproducing the normalized dynamic heat capacity of the material in the vicinity of the glass transition from the TSDC results. The experimental heat capacity measurements can be normalized using:

$$C_p^n = \frac{C_p - C_{pg}}{C_{SmA} - C_{pg}} \tag{5}$$

where C_{pg} is the heat capacity of the smA glassy state and C_{SmA} is the heat capacity of the supercooled smectic A state just when the glass transiton is considered to be finished.

The obtained TSDC curves are the dielectric signature of the glass transition and it is assumed that the dielectric relaxation time is, simply, the relaxation time of the structural relaxation. It is possible to reproduce the calorimetric response of the material [25] by means of the following relationship [42]

$$C_p^n = \frac{dT_f}{dT} \tag{6}$$

where T_f is the fictive temperature. In the modeling $T_f(T)$ is obtained individually for each elementary contribution of the relaxation. The normalized heat capacity of the overall glass transition is the weighted average of the normalized heat capacity of each contribution (obtained by equation 6). The weight of each one is evaluated by the product of the area of the discharge peak and the polarization temperature [36]. We must take into account that the pyrene group is considerably bulkier than the cyanobiphenyl group and, as was discussed previously, it recovers movility at the high temperature glass transition (m_{1L}). This leads to a much larger calorimetric response for the m_{1L} relaxation than for the $m_2 + m_{1H}$ relaxation as was observed experimentally for CBO11O.Py in a previous work [21].

In figure 14 we compare the normalized heat capacity (C_p^n) of CBO9O.py for both the m_{1L} and the $m_2 + m_{1H}$ relaxations, calculated from equation 6, with dynamic heat capacity data measured by means of the MDSC technique and normalized according to equation 5.

With regards to the m_{1L} relaxation, the glass transition temperature of the endothermic peak at the end of the glass transition is approximately reproduced. Instead, the calculated endothermic peak returns to its equilibrium value slower than in the experimental case and its maximum value is overestimated. In the calculated heat capacity a broad exothermic peak can be observed just before the glass transition. This peak appears because the low temperature contributions of the RMA spectra have not been used in the calculations as they appear overlapped to the high temperature contributions of the $m_2 + m_{1H}$ relaxation. In calculations with a proper number of modes this peak disappears when the low temperature contributions are taken into account [25].

On the other hand we can observe that the $m_2 + m_{1H}$ relaxation does not match the experimental data because of its much lower response. Nevertheless, a shoulder in the experimental data (marked with an arrow in figure 14) seems to match the predicted temperature and, as a consequence, it could be due to the contribution of this relaxation to the signal.

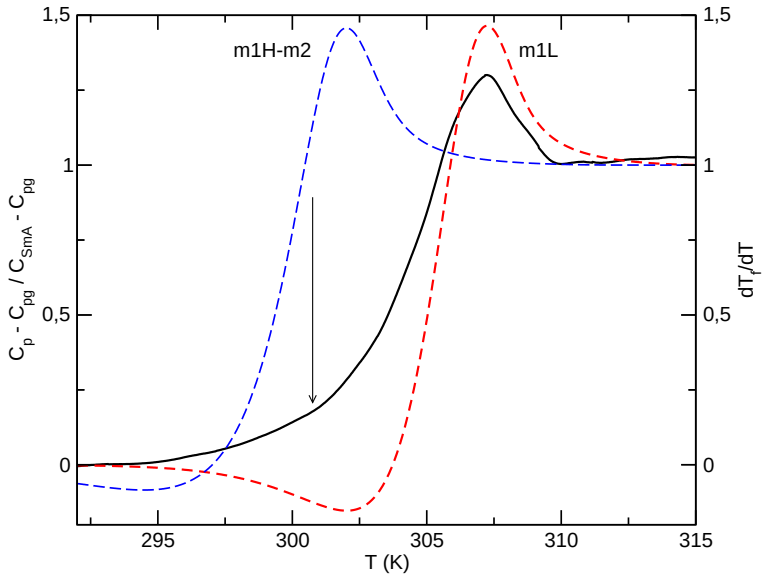

Figure 14. C_p^n for CBO9O.Py at 2 K/min cooling and heating heating rate: experimental (continuous), calculated m_{1L} (dashed) and calculated $m_2 + m_{1H}$ (long-dashed).

4. Conclusions

In this paper we have investigated the dielectric properties of the odd non-symmetric dimers (CBOnO.Py, with n ranging from 3 to 9) in the supercooled mesophases by TSDC and BDS measurements at temperatures very close to the dynamic glass transition. Previous results with CBO11O.Py showed that the different molecular motions of the LC dimer do not lead to a unique glass transition as temperature approaches the glassy state. The main purpose of the present work was to extend the study of the aforementioned molecular motions to the rest of the members of the series.

A clear different behavior has been observed between CBO3O.Py and the rest of the LC dimers of the series. For CBOnO.Py with $n = 5$, 7, 9 an unfolded glass transition is detected in all the cases. TSDC measurements at different thermal and poling conditions allow us to associate the high temperature glass transition with those motions identified by the m_{1L}.

Temperature difference, ΔT, between both glass transitions slightly increases with the spacer n. Measured values are 4.5 K for $n = 5$ and 5.5 K or $n = 7$ and $n = 9$, in good agreement with previous results obtained for CBO11O.Py [21]. BDS measurements in the low frequency range corroborate these results and show that the low temperature relaxation emerges from the superposition of the m_2 and m_{1H} relaxations proposed by Stocchero et al. [20] as the temperature approaches the glass transition. The high temperature glass transition corresponds to m_{1L} that remains as a separated relaxation in all the studied frequency range.

In the case of CBO3O.Py only one glass transition is observed. This behavior could be explained assuming that both relaxations are highly coupled due to the short spacer lenght n in this LC dimer. This prevents the low temperature relaxation to take place until temperature reaches the second glass transition temperature. No effects have been observed associated to the fact that the LC dimers of this series can crystallize in a nematic ($n = 3$, 11) or smectic A ($n = 5$, 7, 9) LC phase.

TSDC measurements, together with partial polarization, allowed us to obtain the Relaxation Map Analysis (RMA) of each transition. RMA results have shown that the first glass transition (m_2+m_{1H}) is more distributed than the second one (m_{1L}) in all the dimers where both relaxations are present ($n = 5$, 7, and 9). Appreciable contributions have been obtained in a wide temperature range of about 15 K for $m_2 + m_{1H}$ and of 9 K for the high temperature relaxation m_{1L}.

Numerical fits of the obtained spectra have shown higher non-linearity in the first glass transition

than the second one. This result has been shown by fitting the obtained spectra to the Tool-Narayanaswamy-Moynihan (TNM). The best results for $m_2 + m_{1H}$ glass transition are obtained with the TNM model with a non-linearity parameter x ranging from 0.92 for CBO5O.Py to 0.8 for CBO9O.Py. This fact indicates that complexity also increases with the flexible spacer length of the LC dimer. On the contrary, the best results in the numerical fits of the second glass transition spectra are obtained, in all the cases, with the TNM model with $x = 1$ that corresponds to the Arrhenius model, fact that indicates that the discharge peak corresponding to m_{1L} is less complex than the other corresponding to $m_2 + m_{1H}$

The normalized heat capacity in the vicinity of the glass transition has been calculated from the fictive temperature ($T_f(T)$) obtained by the TNM model. Numerical simulations from the obtained kinetic parameters show reasonable agreement with measured experimental behaviour.

Acknowledgements

This work has been partially supported by the spanish government (MINECO/FEDER: MAT2015-66208-C3-2-P).

References

[1] Sage IC, Crossland WA, Wilkinson TD, et al. Applications. In: Demus D, Goodby JW, Gray GW, et al., editors. Handbook of liquid crystals. 1st ed. Vol. 1; Weinheim: Wiley-VCH; 1998. p. 731–895.

[2] Patel JS, Lee SD. Fast linear electro-optic effect based on cholesteric liquid crystals. J Appl Phys. 1989; 66(4):1879–1881.

[3] Morris SM, Clarke MJ, Blatch AE, et al. Structure-flexoelastic properties of bimesogenic liquid crystals. Phys Rev E. 2007;75(4):041701(9p).

[4] Imrie CT, Luckhurst GR. Liquid crystal dimers and oligomers. In: Demus D, Goodby JW, Gray GW, et al., editors. Handbook of liquid crystals. 1st ed. Vol. 2B; Weinheim: Wiley-VCH; 1998. p. 801–834.

[5] Imrie CT, Henderson PA. Liquid crystal dimers and higher oligomers: Between monomers and polymers. Chem Soc Rev. 2007;36(12):2096–2124.

[6] Luckhurst GR, Romano S. Computer simulation studies of anisotropic systems. XXVI. liquid crystal dimers: A generic model. J Chem Phys. 1997;107(7):2557–2572.

[7] Šepelj M, Lesac A, Baumeister U, et al. Intercalated liquid-crystalline phases formed by symmetric dimers with an α,ω-diiminoalkylene spacer. J Mater Chem. 2007;17(12):1154–1165.

[8] Sebastián N, De La Fuente MR, López DO, et al. Dielectric and thermodynamic study on the liquid crystal dimer α-(4-cyanobiphenyl-4´-oxy)-ω-(1-pyreniminebenzylidene-4´-oxy)undecane (CBO11O.Py). J Phys Chem B. 2011;115(32):9766–9775.

[9] Cestari M, Frezza E, Ferrarini A, et al. Crucial role of molecular curvature for the bend elastic and flexoelectric properties of liquid crystals: Mesogenic dimers as a case study. J Mater Chem. 2011; 21(33):12303–12308.

[10] Cestari M, Diez-Berart S, Dunmur DA, et al. Phase behavior and properties of the liquid-crystal dimer 1´´, 7´´-bis (4-cyanobiphenyl-4´-yl) heptane: A twist–bend nematic liquid crystal. Physical Review E. 2011;84(3):031704(20p).

[11] López DO, Sebastián N, De La Fuente MR, et al. Disentangling molecular motions involved in the glass transition of a twist-bend nematic liquid crystal through dielectric studies. J Chem Phys. 2012; 137(3):034502(10p).

[12] Sebastián N, López DO, Robles-Hernández B, et al. Dielectric, calorimetric and mesophase properties of 1´´-(2´,4-difluorobiphenyl-4´-yloxy)-9´´-(4-cyanobiphenyl-4´-yloxy)nonane: an odd liquid crystal dimer with a monotropic mesophase having the characteristics of a twist–bend nematic phase. Phys Chem Chem Phys. 2014;16:21391–21406.

[13] Robles-Hernández B, Sebastián N, de la Fuente MR, et al. Twist, tilt, and orientational order at the nematic to twist–bend nematic phase transition of 1,9-bis(4-cyanobiphenyl-4-yl) nonane: A dielectric, 2H NMR, and calorimetric study. Phys Rev E. 2015;92:062505(16p).

[14] López DO, Robles-Hernàndez B, Salud J, et al. Miscibility studies of two twist–bend nematic liquid crystal dimers with different average molecular curvatures. a comparison between experimental data and predictions of a landau mean–field theory for the n-tb-n phase transition. Phys Chem Chem Phys. 2016;18:4394–4404.
[15] Borshch V, Kim YK, Xiang J, et al. Nematic twist-bend phase with nanoscale modulation of molecular orientation. Nat Commun. 2013;4:3635(8p).
[16] Greco C, Luckhurst G, Ferrarini A. Molecular geometry, twist-bend nematic phase and unconventional elasticity: A generalised maier-saupe theory. Soft Matter. 2014;10(46):9318–9323.
[17] Mandle R, Davis E, Voll CC, et al. The relationship between molecular structure and the incidence of the NTB phase. Liq Cryst. 2015;42(5-6):688–703.
[18] Jansze S, Martínez-Felipe A, Storey J, et al. A twist-bend nematic phase driven by hydrogen bonding. Angew Chem Int Edit. 2015;54(2):643–646.
[19] Paterson D, Gao M, Kim YK, et al. Understanding the twist-bend nematic phase: The characterisation of 1-(4-cyanobiphenyl-4´-yloxy)-6-(4-cyanobiphenyl-4´-yl)hexane (cb6ocb) and comparison with cb7cb. Soft Matter. 2016;12(32):6827–6840.
[20] Stocchero M, Ferrarini A, Moro GJ, et al. Molecular theory of dielectric relaxation in nematic dimers. J Chem Phys. 2004;121(16):8079–8097.
[21] Diez-Berart S, López DO, Salud J, et al. Two glass transitions associated to different dynamic disorders in the nematic glassy state of a non-symmetric liquid crystal dimer dopped with γ-alumina nanoparticles. Materials. 2015;8(6):3334–3351.
[22] Sebastián N, De La Fuente MR, López DO, et al. Overall dielectric study on the odd members of a highly nonsymmetric pyrene-based series of liquid crystal dimers. J Phys Chem B. 2013;117(46):14486–14496.
[23] Nordio PL, Rigatti G, Segre U. Dielectric-relaxation theory in nematic liquids. Mol Phys. 1973;25:129–136.
[24] Van Turnhout J. Thermally stimulated discharge of electrets. In: Sessler GM, editor. Electrets. 3rd ed. Vol. 1; Chapter 3; Morgan Hill (CA): Laplacian; 1999. p. 81–215.
[25] Diego JA, Sellarès J, Aragoneses A, et al. TSDC study of the glass transition: Correlation with calorimetric data. J Phys D Appl Phys. 2007;40(4):1138–1145.
[26] Sellarès J, Diego JA, Cañadas JC, et al. Dielectric study of the glass transition of PET/PEN blends. J Phys D Appl Phys. 2012;45(50):505301(13p).
[27] Dargent E, Cabot C, Saiter JM, et al. The glass transition: Correlation of DSC and TSDC investigations. J Therm Anal. 1996;47(3):887–896.
[28] Colomer P, Montserrat S, Pujal M, et al. The glass transition temperature of amorphous poly(ethylene terephthalate) by thermally stimulated currents. J Macromol Sci B. 1984;23(4-6):467–481.
[29] Attard GS, Imrie CT, Karasz FE. Low molar mass liquid-crystalline glasses: Preparation and properties of the α-(4-cyanobiphenyl-4´-oxy)-ω-(1-pyreniminebenzylidene-4´-oxy)alkanes. Chem Mater. 1992; 4(6):1246–1253.
[30] Chen R, Kirsh Y. The analysis of thermally stimulated processes. 1st ed. Oxford: Pergamon; 2013.
[31] Van Turnhout J. Thermally stimulated discharge of polymer electrets. Amsterdam: Elsevier; 1975. Chapter 3; p. 83–96.
[32] Zielinski M, Kryszewski M. Thermal sampling technique for the thermally stimulated discharge in polymers. Phys status Solidi A. 1977;42(1):305–314.
[33] Teyssedre G, Lacabanne C. Some considerations about the analysis of thermostimulated depolarization peaks. J Phys D Appl Phys. 1995;28(7):1478–1487.
[34] Cañadas JC, Diego JA, Mudarra M, et al. Comparative TSPC, TSDC and DSC physical ageing studies on PET-a. Polymer. 1998;39(13):2795–2801.
[35] Diego JA, Belana J, Orrit J, et al. Annealing effect on the conductivity of XLPE insulation in power cable. IEEE T Dielect El In. 2011;18(5):1554–1561.
[36] Teyssedre G, Mezghani S, Bernes A, et al. Thermally stimulated currents of polymers. In: Runt JP, Fitzgerald JJ, editors. Dielectric spectroscopy of polymeric materials. fundamentals and applications. Chapter 8; Washington (DC): American Chemical Society; 1999. p. 227–258.
[37] Tamayo I, Belana J, Cañadas JC, et al. Thermally stimulated depolarization currents of crosslinked polyethylene relaxations in the fusion range of temperatures. J Polym Sci Pol Phys. 2003;41(12):1412–1421.
[38] Cañadas JC, Diego JA, Sellarès J, et al. Comparative study of amorphous and partially crystalline poly(ethylene-2,6-naphthalene dicarboxylate) by TSDC, DEA, DMA and DSC. Polymer. 2000;

41(8):2899–2905.
[39] Puertas R, Rute MA, Salud J, et al. Thermodynamic, crystallographic, and dielectric study of the nature of glass transitions in cyclo-octanol. Phys Rev B. 2004;69(22):224202(9p).
[40] Cusmin P, De La Fuente MR, Salud J, et al. Critical behavior and scaling relationships at the SmAα-N and N-I transitions in nonyloxycyanobiphenyl (9OCB). J Phys Chem B. 2007;111(30):8974–8984.
[41] Cañadas JC, Diego JA, Mudarra M, et al. Relaxational study of poly(ethylene-2,6-naphthalene dicarboxylate) by TSDC, DEA and DMA. Polymer. 1999;40(5):1181–1190.
[42] Hodge IM, Berens AR. Calculation of the effects of annealing on sub-Tg endotherms. Macromolecules. 1981;14(5):1598–1599.